https://doi.org/10.1007/s41230-024-3018-9

Interfacial reaction between AZ91D magnesium alloy melt and mild steel under high temperature

**Jia-hong Dai[1, 2, 3, 4], Jian-yue Zhang[5], *Bin Jiang[2], Xiang-jun Xu[1], Zhong-tao Jiang[6], Hong-mei Xie[1], Qing-shan Yang[7], and Guo-qing Zhang[1, 3]

1. College of Materials Science and Engineering, Yangtze Normal University, Chongqing 408100, China
2. National Engineering Research Center for Magnesium Alloys, College of Materials Science and Engineering, Chongqing University, Chongqing 400044, China
3. Chongqing Jiulongyuan High-tech Industry Group Co., Ltd., Chongqing 400080, China
4. Loncin Industry Co., Ltd., Chongqing 400080, China
5. Department of Materials Science and Engineering, The Ohio State University, Columbus, OH 43210, USA
6. Chongqing Key Laboratory of Materials Surface & Interface Science, Chongqing University of Arts and Sciences, Chongqing 402160, China
7. School of Metallurgy and Material Engineering, Chongqing University of Science and Technology, Chongqing 401331, China

Abstract: The metallurgical quality control of magnesium (Mg) and Mg alloys in melting process is required to ensure a satisfied mechanical and corrosion performance, while the typical used steel crucible introduces impurities and interfacial interaction during melting process. Therefore, a systematic study about impurities diffusion and interfacial interaction between molten Mg and steel is necessary. In the present study, the interfacial reaction between molten AZ91D Mg alloy and mild steel during melting process was investigated with the melting temperatures of 700 °C, 750 °C and 800 °C. The results show that Al(Fe, Mn) intermetallic layer is the intermetallic primarily formed at the interfaces of AZ91D melt and mild steel. Meanwhile, $Al_8(Mn, Fe)_5$ is indexed between Al(Fe, Mn) and AZ91D. $AlFe_3C$ appears between the mild steel and Al(Fe, Mn) at 700 °C and 750 °C, but absent at 800 °C due to the increased solubility of carbon in Mg matrix. It is found that the growth of the intermetallic layer is controlled by diffusion mechanism, and Al and Mn are the dominant diffusing species in the whole interfacial reaction process. By measuring the thickness of different layers, the growth constant was calculated. It increases from $1.89(\pm0.03)\times10^{-12}$ $m^2\cdot s^{-1}$ at 700 °C to $3.05(\pm0.05)\times10^{-12}$ $m^2\cdot s^{-1}$ at 750 °C, and $5.18(\pm0.05)\times10^{-12}$ $m^2\cdot s^{-1}$ at 800 °C. Meanwhile, the content of Fe is linearly increased in AZ91D with the increase of holding time at 700 °C and 750 °C, while it shows a significantly increment after holding for 8 h at 800 °C, indicating holding temperature is more crucial to determine the Fe content of AZ91D than holding time.

Keywords: AZ91D; mild steel; interface reaction; intermetallic growth; kinetics

CLC numbers: TG146.22 **Document code:** A **Article ID:** 1672-6421(2024)02-159-09

1 Introduction

Magnesium (Mg) and Mg alloys are widely recognized as important structural materials for reducing the weight and fuel consumption of vehicles, high-speed trains, and aircrafts owing to their low density and high specific strength [1-3]. The mechanical performance of Mg alloys is strongly influenced by the metallurgical quality achieved during the melting process [4, 5]. For example, the presence of high iron (Fe) content in magnesium alloys can lead to the formation of Fe-containing intermetallics, which negatively impact the mechanical performance. Meanwhile, the high content of Fe will also greatly reduce the corrosion resistance of the alloys [6-12]. Therefore, it is crucial to improve the melting process and ensure high metallurgical quality in Mg production.

During the melting process of Mg, mild steel crucibles are generally used due to the low solubility of Fe in Mg liquid [13-16]. Meanwhile, the Fe content in Mg alloys can be controlled by alloying, and manganese (Mn) is considered the most promising one due to its low cost [17-19]. However, Mn can react with Fe in Mg alloys at high temperatures, especially in AM and AZ systems, which

*Bin Jiang
Male, Ph.D., Professor. His research interests mainly focus on new magnesium alloys and their processing technologies.
E-mail: jiangbinrong@cqu.edu.cn
**Jia-hong Dai
E-mail: daijiahong@yznu.edu.cn
Received: 2023-02-07; Accepted: 2023-08-28

produces Al-Fe(-Mn) intermetallics [20-23]. Simultaneously, Fe element in the crucible may diffuse into the Mg melt [15, 24-27], thus leading to significant changes in alloy composition. In addition, the interfacial reaction leads to the gradual erosion of the crucible, which reduces its service life [15]. A good control of the interfacial reaction between Mg liquid and iron or steel is of vital importance.

Pierre et al. [28] conducted a study on the chemical interaction between mild steel and liquid Mg-Mn alloys at 727 ºC. The results revealed the formation of a transition zone with a gradient in Mn concentration, consisting of an inner layer of α-Fe(Mn) and an outer layer of γ-(Fe, Mn). This transition zone grew at a slow rate through solid-state diffusion. Dai et al. [24] investigated the effect of Mn on the diffusion behavior of Fe in molten Mg and Mg-Mn alloys using diffusion couple method at the temperatures of 720, 760, and 800 °C. At the interface of the Fe/(Mg-2Mn) diffusion couple, a transition layer composed of β-Mn(Fe) and γ-(Fe, Mn) was formed. This transition layer acted as an effective barrier, preventing the diffusion of Fe atoms into molten liquid. Taninouchi et al. [27, 29-30] characterized the interfaces between Mg alloy and SUS316 crucibles. After heat treatment, a Ni-depleted layer was formed on the inner wall due to the preferential dissolution of Ni over Fe and Cr. Scharf et al. [15] calculated the amount of precipitates formed in a steel crucible based on the influence of temperature changes, and determined the equilibrium phases of the AZ91 and AS31 melts. Additionally, they estimated the lifespan of the crucible by assuming a parabolic growth law for the crucible wall thickness. Peng et al. [16] systematically studied the effect of carbon content in Fe-(0-3.6%)C alloys on the interfacial reaction between Fe-(0-3.6%)C and AZ91 alloy. They observed the formation of $AlFe_3C$ and Al_2MgC_2 compounds at temperatures ranging from 700 to 800 ºC. It should be mentioned that the previous studies have primarily focused on thermodynamic aspect. However, the dissolution of Fe and the growth of interfacial layers between Mg liquid and Fe are more kinetically related, particularly at high temperatures. There is currently a shortage of comprehensive studies on this topic. Hence, it is crucial to investigate the kinetic interface reaction between the Mg melt and mild steel crucible during the melting process.

In the present study, the interfacial reaction between AZ91D Mg alloy and mild steel crucibles was investigated. The kinetics of the interfacial reaction were studied at temperatures ranging from 700 to 800 °C, with holding times varying from 4 to 16 h. The microstructure, diffusion behavior of the elements, and growth kinetics of the intermetallics layers at the interfaces between AZ91D and mild steel crucibles were systematically studied.

2 Experimental procedure

The compositions of the commercial AZ91D and mild steel were measured utilizing the inductively coupled plasma-optical emission spectroscopy (ICP-OES), and the results are listed in Table 1. For making the diffusion couple, the AZ91D was fabricated into rods with a diameter of 14.5 mm and length of 32 mm using wire electrical discharge machining (EDM). Mild steel rods were machined into crucibles with an outer diameter of 20 mm, an inner diameter of 15 mm, and a depth of 30 mm. The experimental apparatus used for melting process is illustrated in Fig. 1(a). The AZ91D rods were placed inside the mild steel crucibles. The crucibles were sealed in quartz ampoules, vacuumed, and backfilled with Ar to avoid oxidization and burning during melting process. Then, the quartz ampoules were placed into a preheated Muffle furnace at 700 °C, 750 °C, and 800 ºC, respectively, and held for 4–16 h. Samples were collected at intervals of every 4 h, as shown in Fig. 1(b).

To characterize the microstructure and the Fe content in AZ91D, samples with thickness of 5 mm were machined by wire EDM in the vertical direction at the center of the crucible axis. Meanwhile, a cylinder with a diameter of 7 mm was cut from the center of AZ91 sample to determine the Fe content

Table 1: Chemical compositions of AZ91D magnesium alloy and mild steel (wt.%)

Alloy	Al	Zn	Mn	Fe	Si	Ni	Cu	Mg	Cr	C	S	P
AZ91D	9.5	0.58	0.25	0.004	0.08	0.001	0.002	Bal.	–	–	–	–
Mild steel	–	–	0.45	Bal.	0.3	0.19	0.20	–	0.19	0.21	0.003	0.0031

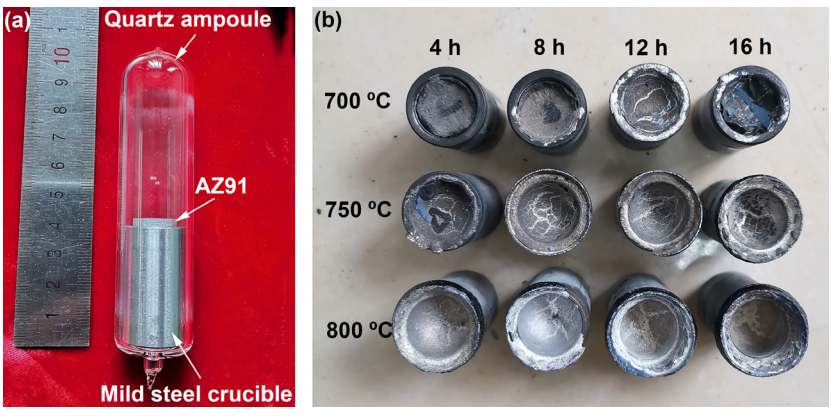

Fig. 1: Experimental apparatus used for melting AZ91D (a), and samples solidified at room temperature (b)

by ICP-OES, as shown in Fig. 2. The sample for interfacial microstructure observation was prepared along cross-section as well. The cross-sections of the mild steel crucibles containing AZ91D were ground and polished to #2000 papers, and etched by 4vol.% nitric acid alcohol solution.

The interfacial cross-section was examined by optical microscopy (OM) and scanning electron microscopy (SEM) equipped with an energy-dispersive X-ray spectroscope (EDS) of Oxford. Elemental distributions were determined by using electron probe microanalysis (EPMA). The thickness of the diffusion layer was determined by averaging the measurements taken at ten different positions within the diffusion layer using SEM images.

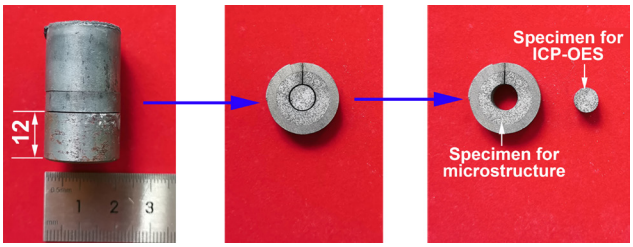

Fig. 2: Sampling position

3 Results and discussion

3.1 Microstructure of interfaces between AZ91D and mild steel crucible

The OM images of the interfaces between AZ91D and mild steel crucible are shown in Fig. 3. The results demonstrate that the number of pearlites in the mild steel crucibles obviously decreases near the interfaces. Meanwhile, a clear decarbonized layer is formed at the surface of mild steel side. This decarbonization is caused by the burning of carbon during the high temperature holding process [32]. The formed intermetallic can be found at the interface while the boundaries of formed intermetallic layers are hard to distinguish from OM.

The formed intermetallic layer between AZ91D and mild steel at the interface was observed by means of back scattered electron (BSE) micrographs, as shown in Fig. 4. It can be clearly found the solidified intermetallic layers at 700 °C and 750 °C. Moreover, numerous black wormlike structures are present in the intermetallic layer at 700 °C and 750 °C, whereas they are absent at 800 °C. For the formed intermetallic layers, the initial steel surface can be found at the mid of interaction region, indicating the formation of intermetallic and the formed intermetallic layer has an atomic contrast close to that of mild steel.

To characterize the intermetallic layer, EDS line scanning of the interfaces between AZ91D and mild steel was conducted for the samples held at 800 °C for 4 to 16 h. Figure 5 indicates the line scanning results. It can be seen Al diffuses from the interface into the interior of the mild steel crucible and its content decreases gradually. Therefore, the thicknesses of the intermetallic layers are approximately 28, 39, 48, 55 μm for samples holding for 4 h, 8 h, 12 h and 16 h, respectively, depending on the dissolution of Al element. The thickness of the intermetallic layers is increased with the increase of holding time.

Figure 6 displays the EDS maps illustrating the atomic distributions of Fe, Al, Mn, Mg, C, and Zn at the interfaces between AZ91D and mild steel after being held at temperatures ranging from 700–800 °C for a duration of 16 h. It is clearly shown that Al and Mn in AZ91D are abundant on the surface of mild steel during melting process. Mg and Zn are uniformly distributed in the AZ91D side. The differences in distribution among them are related to their formation heat with Fe. The formation heat of Fe-Al ($\Delta H^{mix}_{Fe\text{-}Al} = -11$ kJ·mol^{-1}) and Fe-Mn ($\Delta H^{mix}_{Fe\text{-}Mn} = 0$ kJ·mol^{-1}) is significantly lower than that of Fe-Mg ($\Delta H^{mix}_{Fe\text{-}Mg} = 18$ kJ·mol^{-1}) and Fe-Zn ($\Delta H^{mix}_{Fe\text{-}Zn} = 4$ kJ·mol^{-1}) [31]. Therefore, Al and Mn are the dominant diffusing species throughout the entire interfacial reaction process, which aligns with our experimental results regarding the interface reaction between AZ63 and galvanized Q235 during composite casting [32]. It is interesting that a clear carbon enrichment is observed near the interface between the AZ91D matrix and mild steel in the samples held at 700 °C and 750 °C. However, this kind of enrichment is not observed in the sample at 800 °C. This can be attributed to the fact that as temperature increases, the solubility of carbon in the Mg matrix also increases [33-34].

From the element distribution results in Figs. 5(d) and Fig. 7, it can be seen that Fe and Al elements show mutations in the interface between AZ91D and mild steel at 700 °C and 750 °C, while their concentrations in the intermetallic layers remains in a relatively stable range. However, at 800 °C, Fe elements show a linear decreasing trend from mild steel matrix to AZ91D matrix, and Al elements also show a linear decreasing trend but from AZ91D matrix to mild steel matrix.

For better analysis the formation mechanism of intermetallic layer, the EPMA quantitative analysis was used to measure the compositions at Positions 1–15 in Fig. 8. The results are listed in Table 2. Based on the localized atomic ratio and

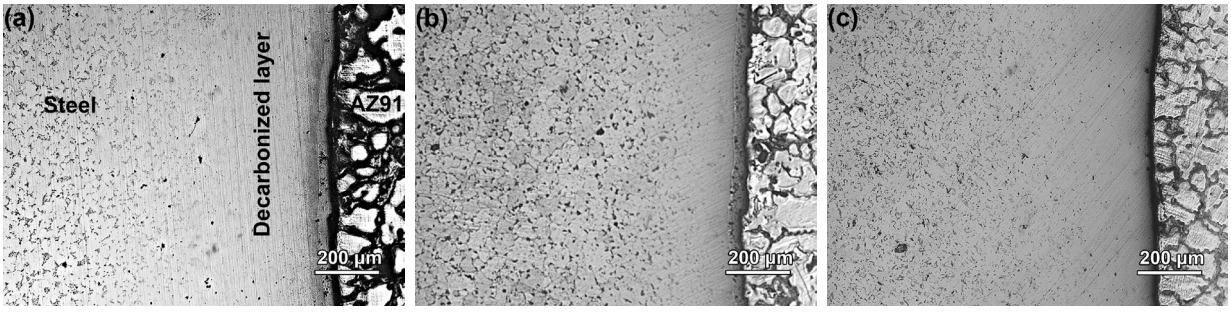

Fig. 3: OM images of interfaces between AZ91D and mild steel held at 700 °C (a), 750 °C (b), and 800 °C (c) for 16 h

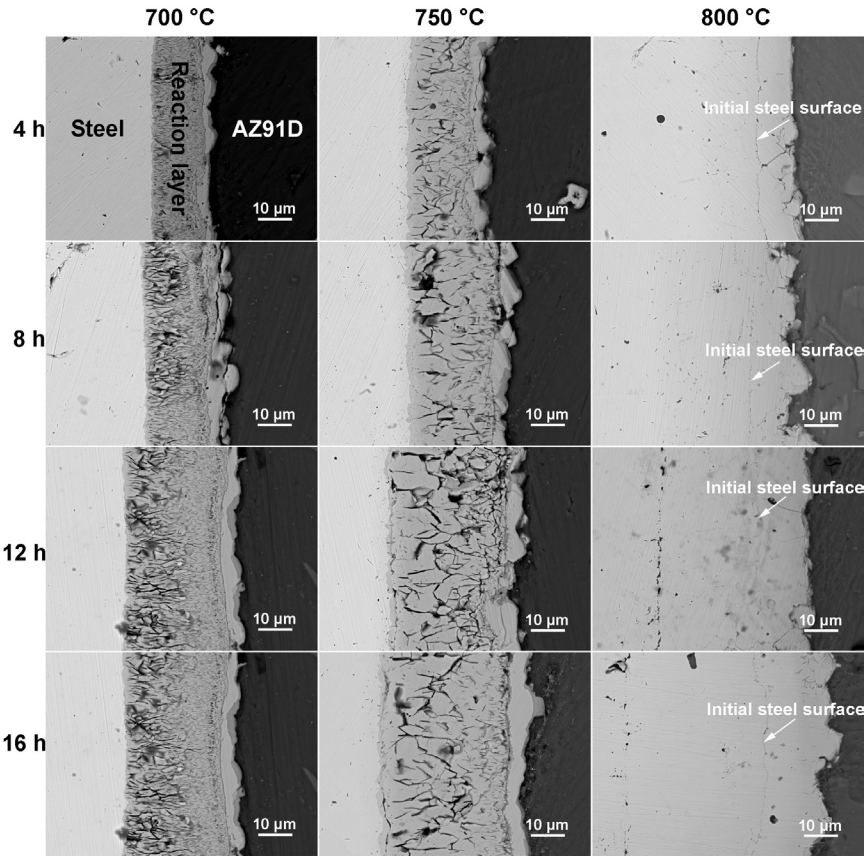

Fig. 4: BSE micrographs of interfaces between AZ91D and mild steel held at 700–800 °C for 4–16 h

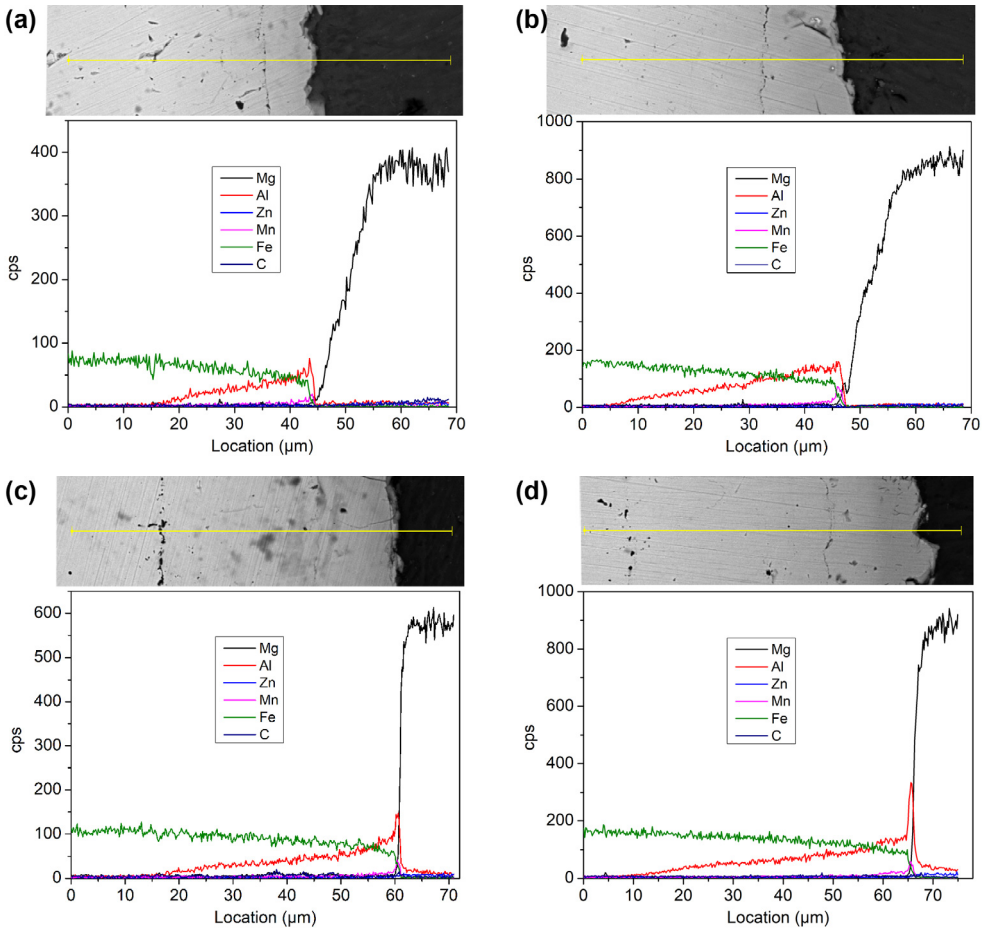

Fig. 5: EDS line scanning of interfaces held at 800 °C for 4 h (a), 8 h (b), 12 h (c), and 16 h (d)

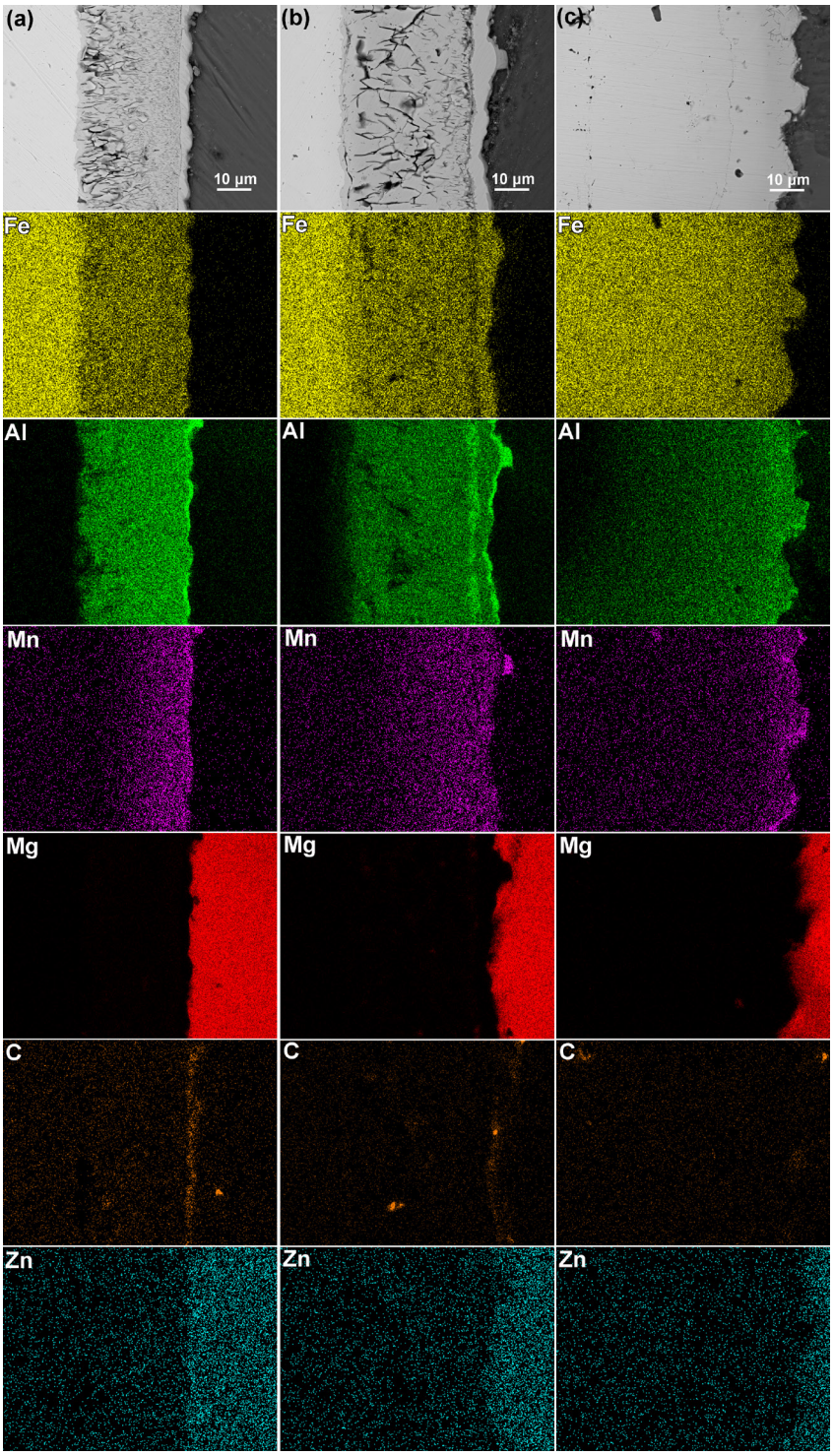

Fig. 6: EDS mapping of interfaces at holding temperature of 700 °C (a), 750 °C (b), and 800 °C (c) for 16 h

the previous report about interface phase formation [9], the corresponding phases of these 15 points can be determined. It can be observed that the intermetallic layer is mainly consisted of Al(Fe, Mn) phases. At 700 °C and 750 °C, numerous thin dark vertical plates are found, which identified as Al_2MgC_2, and some cracks appear. A layer consists of $Al_8(Mn, Fe)_5$ is formed at the bottom of the Al(Fe, Mn) layer. Additionally, there is a thin layer of $AlFe_3C$ between the Al(Fe, Mn) and Fe layers at 700 °C and 750 °C; however, this layer is absent at 800 °C. During initial stages of the experiment at 700 °C and 750 °C, sufficient aluminum beyond its local solubility in Fe diffuses into steel due to decarburization of the mild steel crucible. This leads to carbon diffusion towards the interface and subsequent formation of an $AlFe_3C$ phase. In contrast, Al has a significantly higher solubility in the mild steel at 800 °C, thus all carbon may have diffused and dissolved into the mild steel before enough Al had diffused into the mild steel. In addition, even though the steel surface undergoes decarburization, it has been observed that the solution of carbon in AZ91D liquid at 800 °C remains high [35, 36]. As a result, the formation of the $AlFe_3C$ phase is not possible at this temperature. Similar findings have been reported for the

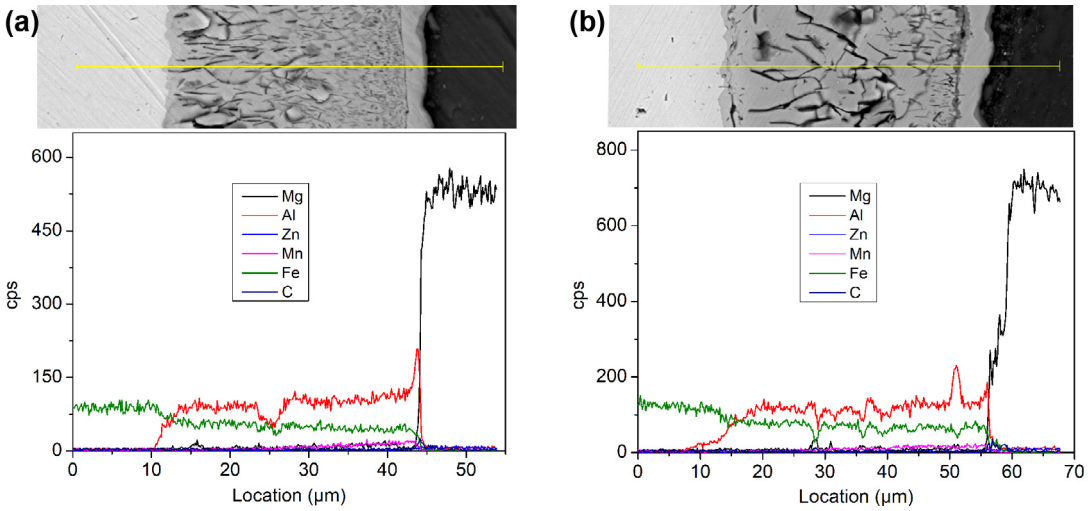

Fig. 7: EDS line scanning of interfaces held at 700 °C (a) and 750 °C (b) for 16 h

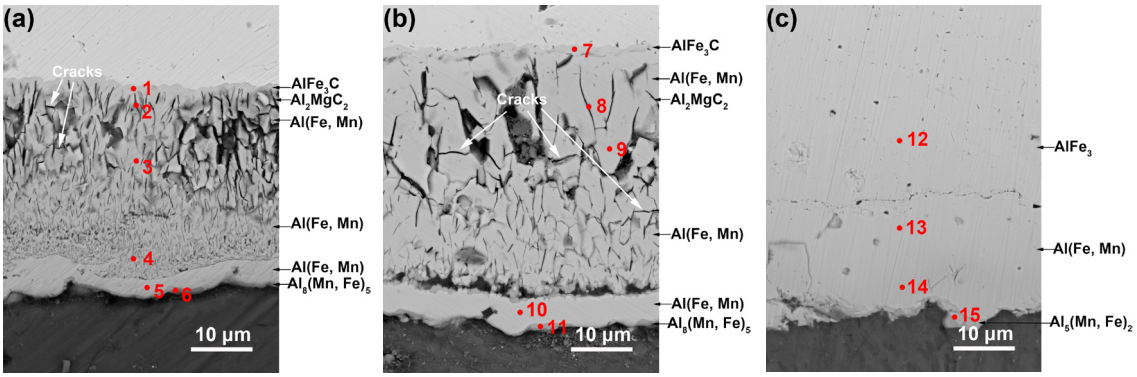

Fig. 8: Microstructures of intermetallic layers held at 700 °C (a), 750 °C (b), and 800 °C (c) for 16 h

Table 2: EPMA results of Points 1–15 in Fig. 8

Point	C (at.%)	Mn (at.%)	Al (at.%)	Fe (at.%)	Mg (at.%)	Phase
1	26.212	0.308	15.837	54.869	2.774	$AlFe_3C$
2	18.684	0.495	37.474	29.742	13.605	Al_2MgC_2
3	3.673	1.918	46.347	47.262	0.8	Al(Fe, Mn)
4	1.871	4.293	49.591	40.578	3.667	Al(Fe, Mn)
5	2.001	10.626	45.623	39.141	2.609	Al(Fe, Mn)
6	1.973	8.144	59.444	27.379	3.06	$Al_8(Mn, Fe)_5$
7	20.721	0.637	19.131	57.219	2.292	$AlFe_3C$
8	16.781	1.269	39.559	32.735	9.656	Al_2MgC_2
9	3.134	6.815	45.625	43.346	1.08	Al(Fe, Mn)
10	2.774	8.802	46.152	42.108	0.164	Al(Fe, Mn)
11	4.001	12.646	57.952	22.898	2.503	$Al_8(Mn, Fe)_5$
12	2.615	1.294	21.023	74.978	0.09	$AlFe_3$
13	6.038	2.868	30.144	60.865	0.085	Al(Fe, Mn)
14	2.945	8.146	45.323	43.411	0.175	Al(Fe, Mn)
15	3.308	7.701	64.537	21.193	3.261	$Al_5(Mn, Fe)_2$

interfacial reaction between Mg melt and carbon steel [9, 37], as well as for hot dip iron-plated carbon alloys on molten aluminum alloys [38-41].

3.2 Growth kinetics of intermetallic layers

The thickness (d) of the intermetallic layer at the interface between AZ91D and mild steel was plotted against the square of time ($t^{1/2}$) for three different temperatures studied, as shown in Fig. 9. The plots shown in Fig. 9 demonstrate a linear relationship between d and $t^{1/2}$, indicating that the growth of intermetallic layers at the interface is controlled by diffusion mechanisms. The data fits perfectly into the parabola:

$$d = \sqrt{kt} \tag{1}$$

where k is the growth constant.

Furthermore, the activation energy (Q) for the intermetallic layers can be estimated by the Arrhenius relation:

$$k = k_0 \exp\left(\frac{-Q}{RT}\right) \tag{2}$$

where k_0 is frequency factor, T is the melting temperature, and R is gas constant. Figure 10 shows the plots of ln$k$ against 1/T. The calculated activation energies and frequency factors from the growth of intermetallic layers are listed in Table 3. It is observed that the growth constant of the intermetallic layer increases with the melting temperature.

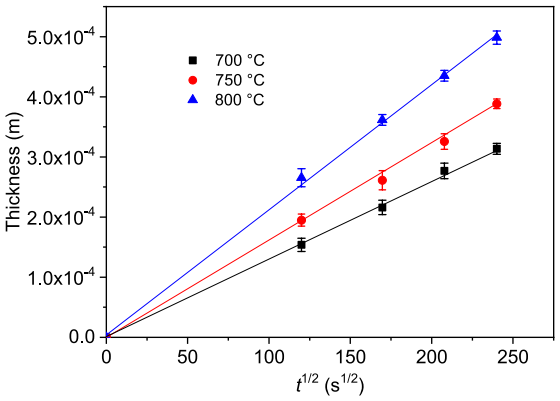

Fig. 9: Growth of intermetallic layers at different temperatures and times

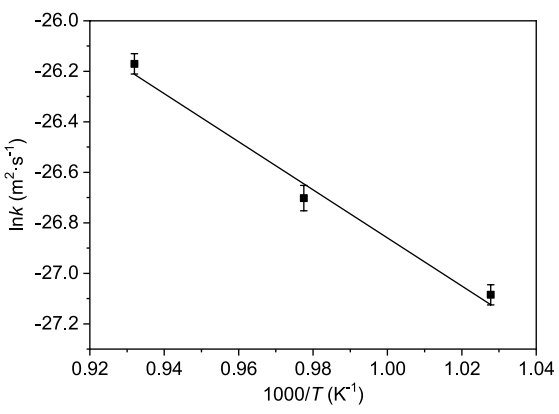

Fig. 10: Arrhenius plot of growth constant k

Table 3: Parameters of growth kinetics for intermetallic layer

T (°C)	k (m²·s⁻¹)	k_0 (m²·s⁻¹)	Q (kJ·mol⁻¹)
700	1.89(±0.03)×10⁻¹²		
750	3.05(±0.05)×10⁻¹²	9.31(±0.59)×10⁻⁸	87.43±4.98
800	5.18(±0.05)×10⁻¹²		

3.3 Analysis of Fe content in AZ91D magnesium alloy

Figure 11 shows the measured Fe content of AZ91D at different temperatures and times. At 700 °C and 750 °C, the Fe content in AZ91D linearly increases with the increase of holding time. Meanwhile, the Fe content becomes higher with the increase of holding temperature. At 800 °C, the Fe content in AZ91D follows a similar trend as at 750 °C when the holding time is less than or equal to 8 h. However, after holding for 8 h, there is a significant increase in Fe content with a further increase in holding time. In summary, increasing the melting temperature and holding time leads to an increase in Fe content in AZ91D. Moreover, it is observed that the holding temperature plays a more crucial role than holding time in determining the Fe content of AZ91D after holding at 800 °C for 8 h.

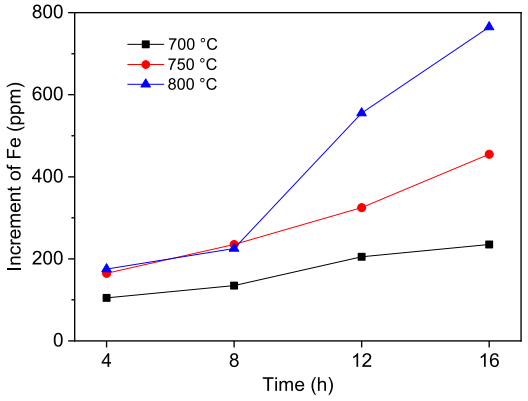

Fig. 11: Changes of Fe content in AZ91D alloy at different temperatures and times

4 Conclusions

In this study, the interface reaction between AZ91D melt and mild steel was investigated at the holding temperatures of 700–800 °C for 4–16 h. The interfacial reaction and the formation of intermetallic layers were kinetically analyzed. The main conclusions are summarized as follows:

(1) During melting and holding process, both Al and Mn in AZ91D are enriched on the surface of mild steel and reacted with Fe to form intermetallic layer. Al and Mn are the dominant diffusing species throughout the interfacial reaction. The concentration of Al in the intermetallic layer remains relatively stable at 700 °C and 750 °C. However, at 800 °C, the concentration of Al in the intermetallic layer decreases linearly from AZ91D to the mild steel crucible matrix.

(2) The formed intermetallics in the reaction layer are predominantly the Al(Fe, Mn) phase, and an $AlFe_3C$ phase is formed near the substrate of mild steel owing to decarburization of the mild steel at 700 °C and 750 ºC. However, the $AlFe_3C$ phase does not form at 800 °C.

(3) The linear fit between the intermetallic layer thickness (d) and square of time ($t^{1/2}$) suggests that the growth of the intermetallic layer is controlled by the diffusion mechanism. At 700 °C, 750 °C and 800 ºC, the growth constants of the intermetallic layer are determined as $1.89(\pm0.03)\times10^{-12}$ $m^2\cdot s^{-1}$, $3.05(\pm0.05)\times10^{-12}$ $m^2\cdot s^{-1}$, and $5.18(\pm0.05)\times10^{-12}$ $m^2\cdot s^{-1}$, respectively. The activation energy Q is 87.43±4.98 $kJ\cdot mol^{-1}$.

(4) As the melting temperature and holding time increase, the Fe content in the AZ91 magnesium alloy linearly increases. However, there is a rapid increase of Fe content at the holding temperature of 800 ºC after 8 h. The result indicates the holding temperature is more crucial to determine the Fe content of AZ91D than holding time after holding at 800 °C for 8 h.

Acknowledgments

This study was supported by the Natural Science Foundation of Chongqing, China (Grant Nos. cstc2020jcyj-msxmX0544, CSTB2022NSCQ-MSX0352, CSTB2022NSCQ-MSX0891, cstc2020jcyj-msxmX0184), Scientific and Technological Research Program of Chongqing Municipal Education Commission (Grant No. KJQN202001416), and National Natural Science Foundation of China (Grant Nos. 11847077, 52001028).

Conflict of interest

The authors declare that they have no known competing financial interests or personal relationships that could have appeared to influence the work reported in this paper.

References

[1] Luo A A. Magnesium casting technology for structural applications. Journal of Magnesium and Alloys, 2013, 1(1): 2–22.
[2] Yang Q, Jiang B, Song B, et al. The effects of orientation control via tension-compression on microstructural evolution and mechanical behavior of AZ31 Mg alloy sheet. Journal of Magnesium and Alloys, 2022, 10(2): 411–422.
[3] Yang H, Chen X, Huang G, et al. Microstructures and mechanical properties of titanium-reinforced magnesium matrix composites: Review and perspective. Journal of Magnesium and Alloys, 2022, 10(9): 2311–2333.
[4] Pan F, Chen X, Yan T, et al. A novel approach to melt purification of magnesium alloys. Journal of Magnesium and Alloys, 2016, 4(1): 8–14.
[5] Prasad A, Uggowitzer P J, Shi Z, et al. Production of high purity magnesium alloys by melt purification with Zr. Advanced Engineering Materials, 2012, 14(7): 477–490.
[6] Pan F S, Mao J J, Chen X H, et al. Influence of impurities on microstructure and mechanical properties of ZK60 magnesium alloy. Transactions of Nonferrous Metals Society of China, 2010, 20(7): 1299–1304.
[7] Chen X H, Mao J J, Pan F S, et al. Influence of impurities on damping properties of ZK60 magnesium alloy. Transactions of Nonferrous Metals Society of China, 2010, 20(7): 1305–1310.
[8] Zhao D, Chen X, Wang X, et al. Effect of impurity reduction on dynamic recrystallization, texture evolution and mechanical anisotropy of rolled AZ31 alloy. Materials Science and Engineering: A, 2020, 773: 138741.
[9] Chen X, Pan F, Mao J, et al. Effect of impurity reduction on rollability of AZ31 magnesium alloy. Journal of Materials Science, 2012, 47(1): 514–520.
[10] Liu M, Uggowitzer P J, Nagasekhar A V, et al. Calculated phase diagrams and the corrosion of die-cast Mg-Al alloys. Corrosion Science, 2009, 51(3): 602–619.
[11] Dai Y, Chen X H, Yan T, et al. Improved corrosion resistance in az61 magnesium alloys induced by impurity reduction. Acta Metallurgica Sinica (English Letters), 2020, 33(2): 225–232.
[12] Liu M, Song G L. Impurity control and corrosion resistance of magnesium-aluminum alloy. Corrosion Science, 2013, 77: 143–150.
[13] Liu F, Hu W, Yang Z, et al. Microstructure evolution and age-hardening response in Mg-Sn-Sm alloys under a wide range of Sm/Sn ratio. China Foundry, 2022, 19(3): 211–217.
[14] Zhang G, Qiu K, Xiang Q, et al. Creep resistance of as-cast Mg-5Al-5Ca-2Sn alloy. China Foundry, 2017, 14(4): 265–271.
[15] Scharf C, Ditze A. Iron pickup of AZ91 and AS31 magnesium melts in steel crucibles. Advanced Engineering Materials, 2007, 9(7): 566–571.
[16] Peng L, Zeng G, Lin C J, et al. Al_2MgC_2 and $AlFe_3C$ formation in AZ91 Mg alloy melted in Fe-C crucibles. Journal of Alloys and Compounds, 2021, 854: 156415.
[17] Gu D D, Peng J, Wang J W, et al. Effect of Mn modification on the corrosion susceptibility of Mg-Mn alloys by magnesium scrap. Acta Metallurgica Sinica (English Letters), 2021, 34(1): 1–11.
[18] Gandel D S, Easton M A, Gibson M A, et al. CALPHAD simulation of the Mg-(Mn, Zr)-Fe system and experimental comparison with as-cast alloy microstructures as relevant to impurity driven corrosion of Mg-alloys. Materials Chemistry and Physics, 2014, 143(3): 1082–1091.
[19] Chen T, Yuan Y, Liu T, et al. Effect of Mn addition on melt purification and Fe tolerance in Mg alloys. JOM, 2021, 73(3): 892–902.
[20] Czerwinski F. Corrosion of materials in liquid magnesium alloys and its prevention. Magnesium alloys–Properties in solid and liquid states. Intech, Rijeka Croatia, 2014: 131–170.
[21] Ohmi T, Iguchi M. Bonding strengths of interfaces between cast Mg-Al alloy and cast-in inserted transition metal cores. Journal of the Japanese Society for Experimental Mechanics, 2013, 13: s189–s193.
[22] Viala J C, Pierre D, Bosselet F, et al. Chemical interaction processes at the interface between mild steel and liquid magnesium of technical grade. Scripta Materialia, 1999, 40(10): 1185–1190.
[23] Nave M D, Dahle A K, Stjohn D H. Method for determining reaction rate of mild steel containers during melting of magnesium-aluminium alloys and effect of aluminium content on directionally solidified microstructures. International Journal of Cast Metals Research, 2003, 16(4): 427–433.
[24] Dai J H, Jiang B, Peng C, et al. Effect of Mn additions on diffusion behavior of Fe in molten magnesium alloys by solid-liquid diffusion couples. Journal of Alloys and Compounds, 2017, 710: 260–266.
[25] Corby C P, Qian M, Ricketts N J, et al. Investigation of intermetallics in magnesium die-casting sludge. Magnesium Technology, 2004: 209–214.

[26] Chen T, Xiong X, Yuan Y, et al. Effect of steels on the purity of molten Mg alloys. Advanced Engineering Materials, 2020, 22(11): 2000338.
[27] Taninouchi Y, Nose K, Okabe T H. Dissolution behavior of iron and steel materials in liquid magnesium. Metallurgical and Materials Transactions: B, 2018, 49(6): 3432–3443.
[28] Pierre D, Viala J C, Peronnet M, et al. Interface reactions between mild steel and liquid Mg-Mn alloys. Materials Science and Engineering: A, 2003, 349: 256–264.
[29] Taninouchi Y, Okabe T H. Solubilities of nickel, iron, and chromium in liquid magnesium in the presence of austenitic stainless steel. Metallurgical and Materials Transactions: B, 2021, 52(2): 611–624.
[30] Taninouchi Y, Yamaguchi T, Okabe T H, et al. Solubility of chromium in liquid magnesium. Metallurgical and Materials Transactions: B, 2022, 53(3): 1851–1857.
[31] Takeuchi A, Inoue A. Classification of bulk metallic glasses by atomic size difference, heat of mixing and period of constituent elements and its application to characterization of the main alloying element. Materials Transactions, 2005, 46(12): 2817–2829.
[32] Dai J, Xie H, Zhou Y, et al. Effect of Q235 hot-dip galvanized and post-casting T6 heat treatment on microstructure and mechanical properties of interfacial between AZ63 and Q235 by solid-liquid compound casting. Metals, 2022, 12(7): 1–12.
[33] Chen H L, Li N, Klostermeier A, et al. Measurement of carbon solubility in magnesium alloys using GD-OES. Journal of Analytical Atomic Spectrometry, 2011, 26(11): 2189–2196.
[34] Chen H L, Schmid-Fetzer R. The Mg-C phase equilibria and their thermodynamic basis. International Journal of Materials Research, 2012, 103(11): 1294–1301.
[35] Okamoto H. The C-Fe (carbon-iron) system. Journal of Phase Equilibria, 1992, 13(5): 543–565.
[36] Chipman J. Thermodynamics and phase diagram of the Fe-C system. Metallurgical and Materials Transactions: B, 1972, 3(1): 55–64.
[37] Nasiri A M, Weckman D C, Zhou Y. Interfacial microstructure of laser brazed AZ31B magnesium to Sn plated steel sheet. Welding Journal, 2015, 94(3): 61S–72S.
[38] Springer H, Kostka A, Payton E J, et al. On the formation and growth of intermetallics phases during interdiffusion between low-carbon steel and aluminum alloys. Acta Materialia, 2011, 59(4): 1586–1600.
[39] Sidhu M S, Bishop C M, Kral M V. Formation of aluminium carbide by cast iron and liquid aluminium interaction. International Journal of Cast Metals Research, 2014, 27(6): 321–328.
[40] Shin D, Lee J Y, Heo H, et al. Formation procedure of reaction phases in Al hot dipping process of steel. Metals, 2018, 8(10): 820.
[41] Kwak S Y, Yun J G, Lee J H, et al. Identification of intermetallics compounds and its formation mechanism in boron steel hot-dipped in Al-7wt.% Mn alloy. Coatings, 2017, 7(12): 1–15.